Additively Manufactured Half-Gutman Lens Antenna for Mobile Satellite Communications

Oskar Zetterstrom, *Graduate Student Member, IEEE*, Nelson J. G. Fonseca, *Senior Member, IEEE*, and Oscar Quevedo-Teruel, *Fellow, IEEE*

***Abstract*—In this letter, we present an additively manufactured half-Gutman lens antenna operating at 30 GHz. The hemispherical lens allows for a compact beamformer while maintaining the wide scanning capabilities of Gutman lenses. This solution further enables to better integrate the feed system when compared to a more conventional half-Luneburg lens antenna design as the focal arc is moved inside the lens. The graded-index of the lens is implemented with a periodic structure arranged in a body-centred cubic (BCC) lattice. We demonstrate that the BCC structure provides attractive properties for the design of inhomogeneous dielectric lenses. Importantly, the BCC structure can be used to alleviate the manufacturing constrains compared to conventional periodic structures. The lens is fed by a dielectric-loaded square waveguide. The proposed antenna produces a directive beam with a simulated and measured peak gain of 26.2 and 25.3 dBi. The antenna can steer its beam in a 50° range in elevation with measured scan loss and sidelobe levels below 1 dB and −10 dB, which agree with the simulated values. The measured cross polarization discrimination is better than 20 dB. The proposed antenna is intended for the ground segment of the emerging low-Earth-orbit satellite communication applications.**

***Index Terms*—Additive manufacturing, body-centred cubic (BCC) lattice, Gutman lens, satellite communications, Wigner–Seitz cell.**

I. Introduction

EMERGING low-Earth-orbit (LEO) satellite communication applications require ground station antennas with a directive beam that can be steered in a wide angular range. The required scanning range is typically 360° in azimuth while the elevation scanning range depends on the application and constellation characteristics (i.e., number of satellites, orbit altitude). In some cases, the elevation scanning is required down to 10°, while for some systems 40–50° is sufficient [1]. In many LEO systems, the operational frequency is high, typically in the K and K_{a}-band. At these frequencies, quasi-optical beamformers [2], and more specifically lenses [3], can provide cost-effective alternatives for directive beam-steering antennas alleviating some of the drawbacks of reflector based solutions.

Manuscript received 22 September 2022; revised 3 November 2022; accepted 21 November 2022. Date of publication 24 November 2022; date of current version 7 April 2023. This work was supported by the ESA ARTES Advanced Technology under Grant 4000125905/18/NL. *(Corresponding author: Oskar Zetterstrom.)*

Oskar Zetterstrom and Oscar Quevedo-Teruel are with the Division of Electromagnetic Engineering, KTH Royal Institute of Technology, SE-100 44 Stockholm, Sweden (e-mail: oskarz@kth.se; oscarqt@kth.se).

Nelson J. G. Fonseca is with the Antenna and Sub-Millimetre Waves Section, European Space Agency, 2200 AG Noordwijk, The Netherlands (e-mail: nelson.fonseca@esa.int).

Digital Object Identifier 10.1109/LAWP.2022.3224455

Rotationally symmetric lens antennas can produce a directive beam that can be steered in a wide angular range with small scan losses [4]. This property can be used to reduce the complexity and cost of the steering mechanisms as only the feed system needs to be actuated. Furthermore, gradient index lenses, such as the Luneburg lens can be aberration-free and can, therefore, provide a high-aperture efficiency [5]. However, the size of the Luneburg lens can be prohibitive for some applications (e.g., mobile satellite communications).

Half-lens antennas have been proposed as a more compact alternative to rotationally symmetric lenses [6], [7], [8]. These lenses are hemispherical, and as a result, the height of the beamformer is reduced by 50%. Half-Maxwell fisheye lens antennas can generate directive beams, but are subject to significant scan losses [6], [9], [10], [11], [12]. Alternatively, a hemispherical Luneburg lens can be placed on a reflective ground plane [13], [14], [15]. The focusing properties of the original beamformer are maintained, however, with reduced scanning range [15], [16]. It is worth noting that in a half-Luneburg lens antenna, the height of the device is increased by the protruding feeding system [13].

Gutman lens antennas can provide similar radiation properties as Luneburg lens antennas [17]. Since the focal point is inside the lens, the feed can be embedded inside the spherical outline of the lens [18]. As a result, half-Gutman lenses possibly allow for a more integrated antenna system. The embedding of the feed comes at a cost of increased required refractive index range in the Gutman lens antenna.

There are no reported works on half-Gutman lens antennas, and the literature on Gutman lens antennas is scarce [19], [20], [21], [22]. In [19], a fully metallic planar Gutman lens antenna is presented. Since the lens is planar, the produced beam is fan-shaped, which is not suitable for the considered application. In [20], a 3-D Gutman lens antenna is presented, which produces a pencil beam. However, the flat feed arrangement (i.e., not following the spherical focal surface) leads to severe scan losses. The impact of the flat feed arrangement is further investigated in [21] and [22], where it is shown to result in increased reflections in the lens [21] and deformed radiation pattern [22].

In this letter, we propose a 3-D half-Gutman lens antenna operating at 30 GHz. The gradient refractive index of the lens is implemented with a periodic structure arranged in a body-centred cubic (BCC) lattice. The lens is realized using fused filament additive manufacturing. The lens is fed with a square waveguide that can be moved along the focal arc so that the

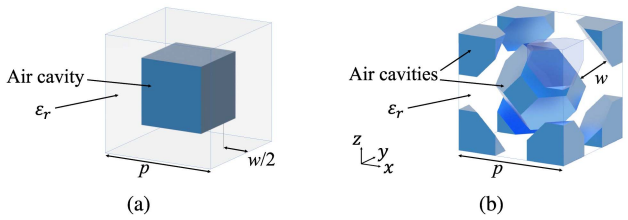

Fig. 1. Unit cells of the studied periodic structures and associated parameters: (a) SC lattice, (b) BCC lattice.

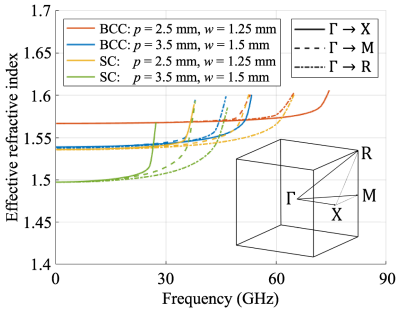

Fig. 2. Effective refractive index as a function of frequency in the studied structures. The permittivity is $\varepsilon_r = 2.6$.

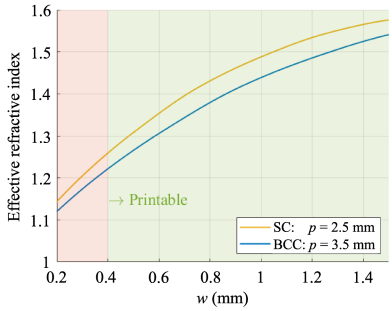

Fig. 3. Effective refractive index at 30 GHz for propagation along the $\Gamma \rightarrow$ X direction for different cavity sizes. The permittivity is $\varepsilon_r = 2.6$.

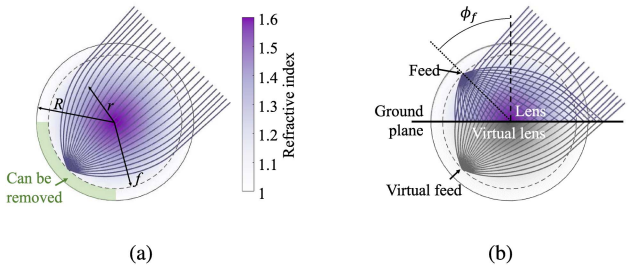

Fig. 4. (a) Refractive index distribution and ray paths in the Gutman lens with $f = 0.8R$. (b) Operation of the half-Gutman lens.

produced pencil beam is steered with small scan losses in a wide range.

II. Unit-Cell Analysis

The refractive index distribution of the Gutman lens is realized in a dielectric medium with air cavities of varying size. This configuration is readily manufactured using fused filament additive manufacturing [20]. Alternative configurations, such as the ones presented in [23], [24], and [25], could be used. However, those structures are either anisotropic (which can affect the scanning performance) or contain narrow pillar-like features (which reduces their mechanical stability).

Two periodic structures are here analyzed and compared. Their unit cells are presented in Fig. 1. The unit cell in Fig. 1(a) corresponds to a periodic structure arranged in a conventional simple cubic (SC) lattice. The unit cell in Fig. 1(b) corresponds to a periodic structure arranged in a BCC lattice. The air cavities are indicated in blue, and have the same shape as the Wigner–Seitz cell of the corresponding lattice. In other words, the cavity shapes are cubical for the SC lattice and truncated octahedral for the BCC lattice. As a result, the periodic structure allows for a large ratio between host material and air without jeopardizing the mechanical integrity as the cavity shapes lead to evenly distributed material thickness. The medium surrounding the air cavities have the permittivity ε_r and the air cavities are scaled uniformly to vary the effective refractive index.

The dispersion diagrams of the structures are obtained using the eigenmode solver in CST. From the dispersion diagram, the effective refractive index is calculated, as presented in Fig. 2. The dimensions are: $p = 2.5$ mm and $w = 1.25$ mm, or $p = 3.5$ mm and $w = 1.5$ mm. The permittivity of the bulk material is $\varepsilon_r = 2.6$. The structures are analyzed for propagation along the three directions that correspond to the edges of the irreducible Brillouin zone, indicated in the inset of Fig. 2. We observe that the BCC structure provides a wider bandwidth for a given periodicity. We note that to operate at 30 GHz, the BCC structure can have a period of 3.5 mm, while the period of the SC structure must be 2.5 mm. A larger period can alleviate the manufacturing.

Fig. 3 presents the effective refractive index at 30 GHz for propagation along the $\Gamma \rightarrow$ X direction for different cavity sizes. We observe that the BCC structure provides a lower effective refractive index for a given wall-width, w. The maximum realizable effective refractive index is the same in both structures, and is obtained when there is no cavity. It is important to note that the range of realizable refractive indices is dictated by the nozzle width of the 3-D printer. As a result, the BCC structure allows for the realization of a larger range of effective refractive indices with a given manufacturing setup.

III. Half-Gutman Lens Antenna

The Gutman lens focuses incident parallel rays to a point inside the lens [17]. The lens is defined by the refractive index distribution

$$n(r) = \sqrt{1 + \left(\frac{R}{f}\right)^2 - \left(\frac{r}{f}\right)^2} \tag{1}$$

where r is the radial position in the lens, R is the radius of the lens, and f is the radius of the focal surface. Fig. 4(a) presents the refractive index distribution and operation of the Gutman lens with $f = 0.8R$. The section behind the focal point [highlighted in green in Fig. 4(a)] can typically be removed without affecting notably the performance. The feeding structure can be placed in

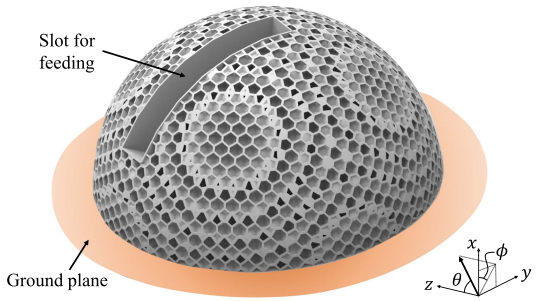

Fig. 5. Illustration of the half-Gutman lens and coordinate system definition.

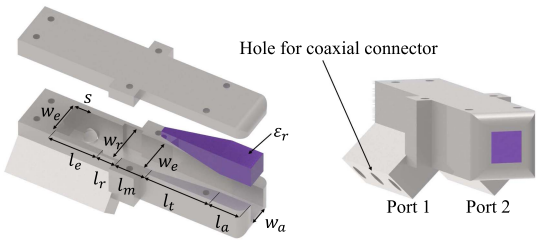

Fig. 6. Illustration of the feeding waveguide and associated design parameters.

Fig. 7. Prototype of the half-Gutman lens antenna.

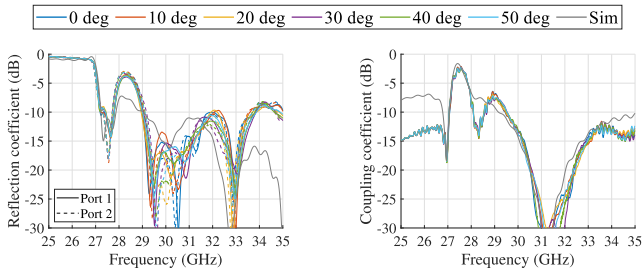

(b) (c)

Fig. 8. Simulated and measured (a) reflection and (b) coupling coefficients as a function of the angular position of the feed, ϕ_f.

the removed section [19]. In this case, the size of the removed section dictates the scanning range of the Gutman lens antenna.

A half-Gutman lens is obtained by placing half of a conventional Gutman lens over a ground plane, as illustrated in Fig. 4(b). The ground plane mirrors the hemispherical lens, producing a virtual half-lens underneath the ground plane [7]. A virtual focal point is observed in the same position as the focal point of a conventional Gutman lens antenna. The focus of the half-Gutman lens is at the mirror position (with respect to the ground plane) of the virtual focus. It is noteworthy that the focusing properties of the original lens are maintained while the size of the beamformer is significantly reduced [7], [13], [26]. The size reduction comes at a cost of reduced scanning range as the half-Gutman lens only provides scanning in half the space. The scanning range in half-Gutman lens antennas is further limited by two factors. First, feeds close to the normal of the ground plane [i.e., at small ϕ_{f} angles as defined in Fig. 4(b)] block the aperture of the antenna, which can result in reduced gain and increased sidelobes [27]. Second, feeds close to the ground plane (i.e., at large ϕ_{f} angles) experience spill-over losses as some rays are not intersecting the ground plane. These spill-over losses result in reduced gain and a secondary lobe in the radiation pattern for the scanned beams. The spill-over losses can be reduced by using a larger ground plane [27], at the cost of increase antenna footprint.

We use the BCC structure to implement a half-Gutman lens. The designed lens is presented in Fig. 5. The focal radius is $f = 0.8R$ and the radius of the lens is $R = 40$ mm (4 wavelengths at 30 GHz). The radius of the ground plane is $1.2R$. Note that the spherical coordinate system used here is not the standard definition for ground terminals, but has been set this way to facilitate the reference to the principal planes in the test setup. The lens is fed by a square waveguide, as illustrated in Fig. 6. The feed has two input ports (accessed through coaxial connectors) that produce orthogonal linearly polarized waves at the output of the feed. The inner conductors of the coaxial connectors protrude 2.75 mm into the waveguide. A dielectric insert ($\varepsilon_r = 2.6$) is placed in the aperture of the feed to reduce the width and decrease the directivity. The widths of the waveguide and dielectric insert are linearly tapered between the dielectric-filled and empty parts. The waveguide has a short section with a rectangular cross-section (of width w_r and length l_r) that is optimized to improve the polarization purity [28]. The dimensions of the feed are as follows: $w_e = 5.5$ mm, $s = 2.7$ mm, $l_e = 7$ mm, $w_r = 5.78$ mm, $l_r = 3$ mm, $l_m = 3$ mm, $l_t = 10$ mm, $l_a = 5$ mm, and $w_a = 3.5$ mm. A slot of width 8 mm is incorporated into the lens to accommodate for the feeding. The feeding slot spans the angular range $-10^\circ \leq \phi_{\mathrm{f}} \leq 60^\circ$, allowing the lens antenna to produce beams in the range $0^\circ \leq \phi \leq 50^\circ$. Note that the angular coverage of the lens antenna is smaller than the angular range of the feeding slot to accommodate for the width of the waveguide. The feeding waveguide protrudes 26 mm outside the lens. Future work will aim at developing a more compact feed that can be fully embedded into the spherical outline of the lens. The prototype of the lens antenna is presented in Fig. 7.

Fig. 8 presents the simulated and measured reflection and coupling coefficients. The measurements are done for different beam pointing directions and the simulation assumes that the feed is radiating into an infinite homogeneous dielectric medium with a permittivity equal to that of the lens at the focal radius. The reflection and coupling coefficients are roughly -15 dB and -13 dB at 30 GHz, and the measurements and simulation agree well. It is worth to note that the bandwidth of the lens is wider than the operational bandwidth of the feed, as indicated in Fig. 2,

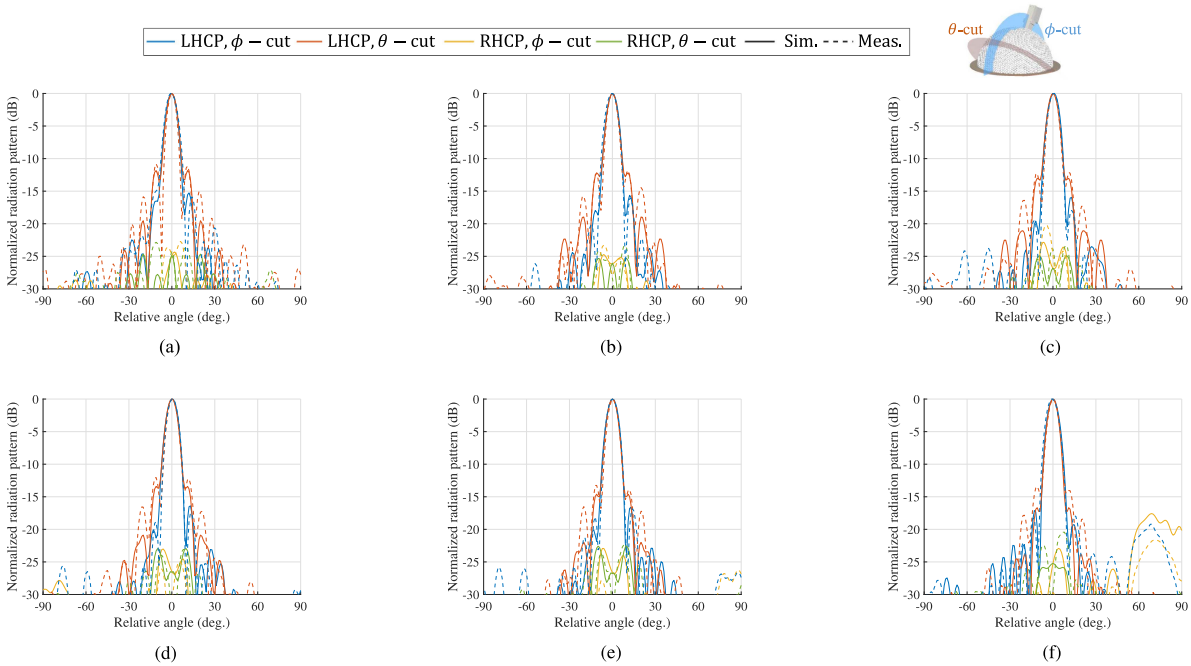

Fig. 9. Simulated and measured normalized radiation pattern in the two main cuts for a beam pointing at $\theta = 90^\circ$ and (a) $\phi = 0^\circ$, (b) $\phi = 10^\circ$, (c) $\phi = 20^\circ$, (d) $\phi = 30^\circ$, (e) $\phi = 40^\circ$, (f) $\phi = 50^\circ$. The relative angle of the abscissa is defined with reference to the pointing direction in the respective cut.

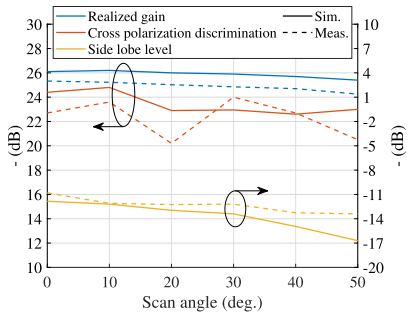

Fig. 10. Simulated and measured peak realized gain, sidelobe levels, and cross-polarization discrimination.

and that a future feed design is intended to provide dual-band operation to cover the uplink and downlink frequency bands.

Fig. 9(a)–(f) presents the normalized radiation pattern of the lens antenna at 30 GHz for beams at $\phi = 0^\circ, 10^\circ, \ldots, 50^\circ$. The linearly polarized far field radiation patterns from the two ports are combined (without considering mutual coupling) into circularly polarized far field patterns in postprocessing. We note that the handedness of the circular polarization is reversed upon reflection on the ground plane. The performance of the lens antenna for different pointing directions is summarized in Fig. 10. The simulated and measured peak gain is 26.2 dBi and 25.3 dBi, and the scan losses are approximately 1 dB. It is noteworthy that the peak gain is observed close to zenith beam pointing, indicating that the effect of the feed blockage is minor. Furthermore, this means that the peak gain of the antenna can be maintained with a smaller ground plane. The simulated and measured sidelobe level is below -10 dB for all beams. The simulated and measured cross polarization discrimination is 20 dB or higher for all beams. The aperture efficiency over the scanning range (with respect to a circular aperture with the same diameter as the lens) is 55%–66% and 43%–54% in simulations and measurements, respectively.

IV. Conclusion

In this letter, we presented a half-Gutman lens antenna operating at 30 GHz that can be additively manufactured using the fused filament fabrication technique. The lens is based on a BCC periodic structure, which is demonstrated to alleviate the manufacturing, compared to a conventional SC periodic structure. Importantly, we show that the BCC structure can realize smaller refractive indices for the same manufacturing resolution, compared to the SC structure. This allows for the realization of a wider range of refractive indices.

For testing purposes, the lens is fed by a dielectric-loaded square waveguide. The waveguide has a short section with a rectangular cross section to improve the polarization purity. Future work will aim at designing a feed that can be fully embedded within the outline of the lens. The proposed lens antenna can steer its directive beam in a 50° elevation range with simulated and measured scan losses and sidelobe levels lower than 1 dB and -10 dB, and cross polarization discrimination higher than 20 dB. The scanning range of the antenna can be increased with a larger ground plane, at the cost of increased in-plane dimensions. The proposed lens is of interest as a user terminal antenna for the emerging LEO satellite constellations.

Acknowledgment

The authors would like to thank the Premix group for supplying the filaments used for the manufacturing of the lens.

REFERENCES

[1] I. del Portillo, B. Cameron, and E. Crawley, "Ground segment architectures for large LEO constellations with feeder links in EHF-bands," in *Proc. IEEE Aerosp. Conf.*, 2018, pp. 1–14.

[2] Y. J. Guo, M. Ansari, R. Ziolkowski, and N. J. G. Fonseca, "Quasi-optical multi-beam antenna technologies for B5G and 6G mm-wave and THz networks: A review," *IEEE Open J. Antennas Propag.*, vol. 2, pp. 807–830, 2021.

[3] O. Quevedo-Teruel, M. Ebrahimpouri, and F. Ghasemifard, "Lens antennas for 5G communications systems," *IEEE Commun. Mag.*, vol. 56, no. 7, pp. 36–41, Jul. 2018.

[4] B. Schoenlinner, X. Wu, J. Ebling, G. Eleftheriades, and G. Rebeiz, "Wide-scan spherical-lens antennas for automotive radars," *IEEE Trans. Microw. Theory Techn.*, vol. 50, no. 9, pp. 2166–2175, Sep. 2002.

[5] R. K. Luneburg and M. Herzberger, *Mathematical Theory of Optics*. Berkeley, CA, USA: Univ. of California Press, 1944.

[6] B. Fuchs, O. Lafond, S. Rondineau, and M. Himdi, "Design and characterization of half Maxwell fish-eye lens antennas in millimeter waves," *IEEE Trans. Microw. Theory Techn.*, vol. 54, no. 6, pp. 2292–2300, Jun. 2006.

[7] J. Thornton, "Wide-scanning multi-layer hemisphere lens antenna for Ka band," *IEE Proc. Microw. Antenn.*, vol. 153, pp. 573–578, Dec. 2006.

[8] J. Thornton and K.-C. Huang, "Hemispherical lens-reflector scanning antennas," in *Proc. Modern Lens Antennas Commun. Eng.*, 2012, pp. 225–266.

[9] Z. L. Mei, J. Bai, T. M. Niu, and T. J. Cui, "A half Maxwell fish-eye lens antenna based on gradient-index metamaterials," *IEEE Trans. Antennas Propag.*, vol. 60, no. 1, pp. 398–401, Jan. 2012.

[10] D. Headland, M. Fujita, and T. Nagatsuma, "Half-Maxwell fisheye lens with photonic crystal waveguide for the integration of terahertz optics," *Opt. Exp.*, vol. 28, no. 2, pp. 2366–2380, Jan. 2020.

[11] H.-T. Chou, H.-J. Su, and H.-J. Huang, "2-D deformed half fisheye lens as beamforming network to excite planar arrays of antennas for multibeam radiations," *IEEE Trans. Antennas Propag.*, vol. 69, no. 11, pp. 7440–7451, Nov. 2021.

[12] J. M. Poyanco, F. Pizarro, and E. Rajo-Iglesias, "3D-printed half-Maxwell fish-eye dielectric lens antenna with integrated DRA feed," in *Proc. 16th Eur. Conf. Antennas Propag.*, 2022, pp. 1–5.

[13] A. R. Weily and N. Nikolic, "Dual-polarized planar feed for low-profile hemispherical Luneburg lens antennas," *IEEE Trans. Antennas Propag.*, vol. 60, no. 1, pp. 402–407, Jan. 2012.

[14] H. Lu, Z. Liu, Y. Liu, H. Ni, and X. Lv, "Compact air-filled Luneburg lens antennas based on almost-parallel plate waveguide loaded with equal-sized metallic posts," *IEEE Trans. Antennas Propag.*, vol. 67, no. 11, pp. 6829–6838, Nov. 2019.

[15] N. J. G. Fonseca, Q. Liao, and O. Quevedo-Teruel, "Compact parallel-plate waveguide half-Luneburg geodesic lens in the Ka-band," *Microw., Antennas Propag.*, vol. 15, no. 2, pp. 123–130, Feb. 2021.

[16] O. Zetterstrom, N. J. Fonseca, and O. Quevedo-Teruel, "Compact half-Luneburg lens antenna based on a glide-symmetric dielectric structure," *IEEE Antennas Wireless Propag. Lett.*, vol. 21, no. 11, pp. 2283–2287, Nov. 2022.

[17] A. S. Gutman, "Modified Luneberg lens," *J. Appl. Phys.*, vol. 25, no. 7, pp. 855–859, 1954.

[18] O. Quevedo-Teruel, W. Tang, and Y. Hao, "Isotropic and nondispersive planar fed Luneburg lens from Hamiltonian transformation optics," *Opt. Lett.*, vol. 37, no. 23, pp. 4850–4852, Dec. 2012.

[19] P. Bantavis, C. G. Gonzalez, R. Sauleau, G. Goussetis, S. Tubau, and H. Legay, "Broadband graded index Gutman lens with a wide field of view utilizing artificial dielectrics: A design methodology," *Opt. Exp.*, vol. 28, no. 10, pp. 14648–14661, May 2020.

[20] O. Bjorkqvist, O. Zetterstrom, and O. Quevedo-Teruel, "Additive manufactured dielectric Gutman lens," *Electron. Lett.*, vol. 55, no. 25, pp. 1318–1320, Dec. 2019.

[21] E. Semernya and S. Skobelev, "Wave focusing analysis in a truncated Gutman lens," *Tech. Phys. Lett.*, vol. 47, no. 11, pp. 773–776, Dec. 2021.

[22] I. Grigoriev and I. Munina, "Multibeam truncated Gutman lens based on additive manufacturing," in *Proc. Int. Workshop Antenna Technol.*, 2022, pp. 104–106.

[23] M. Liang, W.-R. Ng, K. Chang, K. Gbele, M. E. Gehm, and H. Xin, "A 3-D Luneburg lens antenna fabricated by polymer jetting rapid prototyping," *IEEE Trans. Antennas Propag.*, vol. 62, no. 4, pp. 1799–1807, Apr. 2014.

[24] Z. Larimore, S. Jensen, A. Good, A. Lu, J. Suarez, and M. Mirotznik, "Additive manufacturing of Luneburg lens antennas using space-filling curves and fused filament fabrication," *IEEE Trans. Antennas Propag.*, vol. 66, no. 6, pp. 2818–2827, Jun. 2018.

[25] C. Wang, J. Wu, and Y.-X. Guo, "A -printed wideband circularly polarized parallel-plate Luneburg lens antenna," *IEEE Trans. Antennas Propag.*, vol. 68, no. 6, pp. 4944–4949, Jun. 2020.

[26] J. Sanford, "A Luneberg-lens update," *IEEE Antennas Propag Mag*, vol. 37, no. 1, pp. 76–79, Feb. 1995.

[27] J. Thornton, "Aperture blockage and truncation in scanning lens-reflector antennas," *Microw., Antennas Propag.*, vol. 4, pp. 828–836, Jul. 2010.

[28] N. J. G. Fonseca, "Two-probe waveguide orthomode transducer with twofold rotational symmetry," *IEEE Trans. Microw. Theory Techn.*, vol. 69, no. 7, pp. 3228–3235, Jul. 2021.